Current Applied Physics 13 (2013) 1037–1041

Contents lists available at SciVerse ScienceDirect

Current Applied Physics

journal homepage: www.elsevier.com/locate/cap

Interfacial electronic structure of molybdenum oxide on the fullerene layer, a potential hole-injecting layer in inverted top-emitting organic light-emitting diodes

J.T. Lim, J.W. Park, G.Y. Yeom*

School of Advanced Materials Science and Engineering, Sungkyunkwan University, Suwon 440-746, Republic of Korea

ARTICLE INFO

Article history:
Received 10 July 2012
Received in revised form
9 January 2013
Accepted 13 February 2013
Available online 14 March 2013

Keywords:
Electronic structure
Inverted top-emitting organic light-emitting diode
Ultraviolet photoemission spectroscopy
X-ray photoemission spectroscopy
Near-edge X-ray absorption fine structure

ABSTRACT

The interfacial electronic structures of molybdenum oxide (MoO_x) deposited on fullerene (C_{60}) which could be used as a hole-injecting layer in inverted top-emitting organic light-emitting diodes (TE-OLEDs) were investigated by photoemission spectroscopy. The hole-injecting barrier height (Φ_B^h) at each interface investigated by an ultraviolet photoemission spectroscopy was reduced to from 1.4 to 0.1 eV as the thickness of MoO_x (Θ_{MoOx}) was increased from 0.1 to 5.0 nm on C_{60}. In these interface system, the sign of vacuum-level shift, highest occupied molecular orbital (HOMO)-level shift, and core-level shifts were all positive indicating that the interface mechanism is attributed to the work-function differences due to a band bending at these interfaces. Moreover, the near-edge X-ray absorption fine structure spectra at carbon K-edge did not show any structural modification as well as any chemical reaction at the MoO_x-on-C_{60} interfaces when Θ_{MoOx} was changed on C_{60}. From these results, the inverted TE-OLED with C_{60} (5.0 nm)/MoO_x (5.0 nm) showed the power efficiency of 1.7 lm/W at a luminance of about 1000 cd/m^2 and the maximum luminance of about 76.000 cd/m^2 at the bias voltage of 11.0 V. It exhibited the highest performance among the inverted TE-OLEDs fabricated as a function of MoO_x thickness from 0 to 5.0 nm.

1. Introduction

Organic light-emitting diode (OLED) display is not only one of the most promising next-generation flat panel displays but also an energy-efficient solid-state lighting source on account of their advantages such as self-emission, a simple structure, a high response speed, and a wide viewing angle [1–3]. For about a decade, active matrix (AM) OLED displays using thin film transistor backplane have been developed for pursing higher resolution and lower power consumption [4]. It had been proved that the top-emission (TE) structure is suitable for high efficiency AM-OLED displays, since the structure allows the designing of a large aperture for high-resolution display, both without being bothered by the pixel circuits and with eliminating light-loss induced by waveguide effect in the glass substrate, which exist in conventional bottom-emission OLEDs [5]. Moreover, the inverted TE-OLED provides an advantage for making use of the n-channel a-Si thin film transistors, which could give more uniform brightness for a large area display.

Meanwhile, the interfaces between electrodes and organic layers are central to the physics of OLEDs, since the mismatch between the Fermi level (E_F) of electrodes and the organic (or inorganic) highest occupied molecular orbital (HOMO) and lowest unoccupied molecular orbital (LUMO) controls the charge injection into the device. More specifically, low work function (Φ) cathodes and high Φ anodes are needed in order to fabricate efficient diodes by minimizing injection barriers [6]. The appropriate aligning of the relevant levels in organic (or inorganic)-electrode contact is necessary to maximize the luminous efficiency and minimize the power consumption by developing a low-voltage carrier-injecting layer. Also, a phenomenon occurring at an organic-electrode contact could be understood by interpreting various interface mechanisms, such as a chemical reaction, interface dipole by charge transfer, an image effect which is formed through either mirror force or surface rearrangement, a formation of either new interface states or permanent dipole, etc [6].

Recently, as *p*-type dopants, transition-metal oxides such as molybdenum oxides (MoO_3) [7–11] tungsten oxides (WO_3) [12], vanadium oxides (V_2O_5) [13], and ReO_3 [14] have been investigated as promising candidates to replace the organic hole injection layers, due to their stability and their high Φ. Among these *p*-type carrier-injecting layers, MoO_3 have been frequently used as

* Corresponding author. Fax: +82 31 299 6565.
E-mail addresses: gyyeom@skku.edu, yeom1485@kornet.net (G.Y. Yeom).

1567-1739/$ – see front matter © 2013 Elsevier B.V. All rights reserved.
http://dx.doi.org/10.1016/j.cap.2013.02.022

a hole-injecting layer (HIL) between a tin-doped indium oxide (ITO) layer and a hole-transporting layer (HTL) [7–11]. The MoO_x-doped HILs and MoO_x/HILs lead to an ohmic contact when inserted at between ITO and the HTL. Numerous studies have been reported to prove the reason why an ohmic contact is formed. It includes a formation of charge transfer complexes [9–11,15,16], a low hole-injecting barrier height (Φ_B^h) and new metal-induced gap states below the E_F at these interfaces [7]. Since a contact between the electrode and the inorganic (or organic) is one of the most important factors in determining the device performance in OLEDs, it is imperative to understand and design the inorganic (or organic)-electrode interface.

In this paper, it was found that the MoO_x-on-fullerene (C_{60}) layers would be potential HILs in inverted TE-OLEDs [17]. The C_{60} layer consisting of HIL was introduced to increase the work function of Al anode. It has been reported that the work function of a metal can be increased by covering a thin layer C_{60} due to the strong redistribution of mobile charge carrier at metal/C_{60} interfaces [18,19], and efficient OLEDs were also fabricated using C_{60} as a HIL [20]. Therefore, in this study, MoO_x-on-C_{60} was investigated as a HIL even though MoO_x itself has been widely used as a HIL for enhancing hole injection in OLEDs [21]. We report on an interface mechanism as well as the Φ_B^h at these interfaces, in which electronic structure was investigated by various photoemission spectroscopic methods. Also, the correlation between the device performance of the inverted TE-OLED and the each interfacial electronic structure was discussed.

2. Experimental

The inverted TE-OLED has a *p*-Si/aluminum (Al, 150 nm)/lithium fluoride (LiF, 1.0 nm)/tris(8-quinolinolato)aluminum (III) (Alq_3, 40.0 nm)/N,N′-diphenyl-N,N′-bis(1-naphthyl)-1,1′-biphenyl-4,4′-diamine (NPB, 60.0 nm)/C_{60} (5.0 nm)/MoO_x (*x* nm)/Al (2.0 nm)/silver (Ag, 18.0 nm)/Alq_3 (52.0 nm) structure. The bottom Al was used as a reflective cathode, LiF as an electron-injecting layer (EIL), bottom Alq_3 both as an electron-transporting layer (ETL) and a green emissive material layer (EML), NPB as a HTL, C_{60}/MoO_x as a HIL, Al/Ag as a semi-transparent anode [22], and top Alq_3 as a capping layer, and they were sequentially vacuum-deposited by using a thermal evaporation system. The thickness of MoO_x (Θ_{MoOx}) on C_{60} in device I, device II, device III, device IV was 0, 0.5, 1.0, and 5.0 nm, respectively. Also, the device V was consisted of 5 nm-thick MoO_x only as a HIL. The emissive active area of the devices was 2×2 mm^2. The top capping layer of Alq_3 (refractive index: 1.7) functions both as a transparent dielectric index-matching layer and as a semi-passivation layer [23]. The current density–voltage–luminance characteristics were measured using a Keithley 2400 electrometer, a photodiode (Oriel 71608), and a Keithley 485 picommeter.

The electronic structures of the MoO_x-on-C_{60} layers were investigated by using X-ray photoemission spectroscopy (XPS), ultraviolet photoemission spectroscopy (UPS), and near-edge X-ray absorption fine structure (NEXAFS) spectroscopy at the 4B1 beam line in the Pohang Accelerator Laboratory (Korea). All measurements and depositions were performed in an ultra-high vacuum system, consisting of a main analysis chamber (approximately 5×10^{-10} Torr) and a sample preparation chamber (approximately 5×10^{-9} Torr). For the analysis, all the samples were prepared *in-situ* via sequential thermal evaporation on a *p*-type Si wafer in an ultra-high vacuum system which was connected to the beam line in vacuum. Also, all thicknesses were determined by timed depositions calibrated using a quartz-crystal microbalance. In the XPS studies, incident photon energies of 350 and 650 eV was used to obtain the core level spectra of carbon (C) 1*s* and oxygen (O) 1*s*, respectively. For the UPS measurements, the He *I* (21.2 eV) line from a UV source was used. The photoemission onset which reflects Φ at the surface of all samples was measured by biasing the samples at −5 V. The incident photon energy was calibrated by measuring the Au 4*f* level of a clean Au surface. In the NEXAFS analyses, C K-edge (270–320 eV) spectra were measured at a photon incident angle of 45.0°.

3. Results and discussion

The metal oxide/organic interfaces (as a HIL) have been found to be critical in determining device performance of organic semiconductor such as OLEDs, organic transistors, and organic bulk hetero-junction solar cells. In an inverted TE-OLED structure, the metal oxide is placed on the organic layer, forming an organic/metal oxide interface [8]. To elucidate the mechanism involved in the light-emitting enhancement of the inverted TE-OLEDs, electronic structures of the MoO_x-on-C_{60} interfaces were investigated by using various photoemission spectroscopic techniques as a function of Θ_{MoOx}. Especially, a robust interface is required with no potential barrier to carriers in order to prevent a Joule heating at the interface [24]. Also, the investigation of the energy levels of the MoO_x-on-C_{60} interfaces is important in understanding the Φ_B^h near the HIL/anode interface of the OLED structure investigated in this study. Fig. 1 shows the evolution of the He *I* valence band (VB) spectra of the pristine C_{60} and MoO_x-on-C_{60} thin films with an incremental Θ_{MoOx}. The MoO_x-on-C_{60} thin films were *in-situ* fabricated by sequentially depositing MoO_x after pre-forming the 10.0 nm-thick C_{60} layer on a *p*-Si wafer. Fig. 1(a) and (b) exhibits the onset of VL representing Φ on the surface and a HOMO region around the E_F of the MoO_x-on-C_{60} layers, respectively. Also, the bar indicates the onset of the VL and HOMO in Fig. 1(a) and (b), respectively. As shown in the bottom curve of Fig. 1(a), the Φ onset of the pristine C_{60} is positioned at 4.7 eV, which is equal to the photon energy (21.2 eV) minus VB width (16.5 eV) [6]. In the bottom curve of Fig. 1(b), the Φ_B^h, which is the energy difference between the E_F of anode and the HOMO edge of pristine C_{60}, is about 1.5 eV. The ionization energy of pristine C_{60}, which is VL (4.7 eV) plus HOMO (1.5 eV), is measured as 6.2 eV in Fig. 1. In addition, the

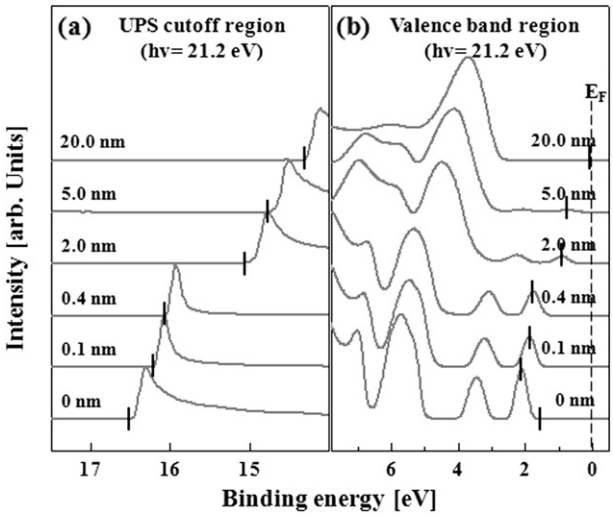

Fig. 1. UPS spectra of the pristine C_{60} and MoO_x-on-C_{60} thin films as a function of Θ_{MoOx} on the 10.0 nm-thick C_{60} layer. (a) shows the onset of VB representing Φ on the surface and (b) shows the valence spectra, at the MoO_x-on-C_{60} interfaces. The values in the figures indicate the thickness of Θ_{MoOx}. Also, the bar indicates the onset of the VL and HOMO in (a) and (b), respectively.

pristine C_{60} has a band gap of about 2.3 eV. It suffices to mention here that our data are in excellent agreement with previously published results [25].

In VB spectra of Fig. 1(b), the HOMO-1 (at around 3.5 eV) and HOMO (at around 2.1 eV) features present in pristine C_{60} film [26]. Although the C_{60} features attenuate with increasing a Θ_{MoOx} on C_{60}, the molecular peaks remain clearly and all molecular levels steadily shift toward the E_F. When the Θ_{MoOx} of 0.1 nm–5.0 nm was deposited on C_{60}, the Φ_B^h between Al anode and the MoO_x-on-C_{60} interfaces were dramatically reduced from 1.3 to 0.1 eV. The decrease of Φ_B^h implies that a hole concentration could be largely increased in the MoO_x-on-C_{60} interfaces. Also, in Fig. 1(a), the Φ at the MoO_x-on-C_{60} interfaces showed the large rising up to 6.9 eV as the Θ_{MoOx} was increased from 0.1 to 5.0 nm, when compared to that of pristine C_{60} (4.7 eV).

Fig. 2(a) shows the XPS C 1*s* electron density curves (EDCs) measured as a function of a Θ_{MoOx} on 10 nm-thick C_{60}. For the pristine C_{60}, the C core-level EDC was symmetrical in shape and was composed of a single component, indicating a clean C_{60} film. For the pristine C_{60}, the peak is located at the binding energy (E_B) of 284.7 eV and is well coincide with the published data of pristine C_{60} [25]. For $\Theta_{MoOx} = 0.1$ nm, the C 1*s* EDC was shifted to a little lower E_B of 284.6 eV and was shifted further to 283.4 eV as the Θ_{MoOx} is increased to 5.0 nm. This peak shift to a lower E_B was caused by a decrease in the Coulomb potential between the nuclei and the electron of the valence band as a result of the increased electron density at the valence band of carbon atoms due to Φ difference. The E_B rising of 1.3 eV with the increase of Θ_{MoOx} from 0 to 5 nm showed the similar trend to the shifts of both the HOMO and Φ levels in Fig. 1. Fig. 2(b) shows XPS O 1*s* core level EDCs as a function of the Θ_{MoOx} on 10.0 nm-thick C_{60}. At the $\Theta_{MoOx} = 0.1$ nm, the symmetrical O 1*s* peak appears at 532.6 eV. As the Θ_{MoOx} was increased from 0.1 to 5.0 nm on C_{60}, the E_B was largely shifted by 2.2 eV toward lower binding energy. Because the signs of the energy shifts are all positive for the EDCs of C and O, it is believed that the E_B shift to a lower energy observed in Fig. 2 is originated from the band bending not from electron charge transfer between C_{60} and MoO_x. This result implies that interface dipole by electron charge transfer is not occurred at these interfaces.

To identify whether additional chemical reactions and/or electron charge transfers occur or not between the MoO_x and C_{60} interfaces, the NEXAFS spectra were investigated. The NEXAFS spectroscopy shows the resonance features induced by the absorption of X-rays that excite electrons from the initial state (core level) to the final state (vacant level) and can be used to obtain information on both the core levels and the unoccupied states. Fig. 3 shows the total electron yield (TEY) NEXAFS spectra, which are measured at the photon incident angle of 45.0°, for the C K-edge of the pristine C_{60} and the MoO_x-on-C_{60} interfaces with increasing the Θ_{MoOx} on C_{60} of 10 nm. The C K-edge $1s \rightarrow \pi^*$ resonances of pristine C_{60} in Fig. 3 were 284.5 (LUMO), 286.3 (LUMO+1 and LUMO+2), and 288.5 eV (LUMO+3), respectively, with allowing a straightforward peak assignment [27]. This alignment means a transition involved to the conjugation of C_{60}. When MoO_x of 0.1–5.0 nm is deposited on C_{60}, the main features of the $1s \rightarrow \pi^*$ energy shift remain clearly unchanged and the intensity change of the π^*-derived exciton peaks is negligible, as deduced by the direct comparison of the spectra for different coverage. This indicates that any structural modification as well as any chemical reaction is not occurred at the MoO_x-on-C_{60} interface because the core level and vacant levels are not changed at TEY-NEXAFS spectra.

Fig. 4 exhibits the onsets of the energy levels (Φ, HOMO, LUMO, and E_B) in the MoO_x-on-C_{60} interfaces, obtained from the results in Figs. 1 and 2. In this interface system, the sign of Φ shift, HOMO-level shift, and core-level shifts are all positive. The large rising of all energy levels are attributed to the work-function differences due to band bending, not being occurred from interfacial dipole effect due to electron charge transfer between MoO_x and C_{60}.

Fig. 5 shows the proposed energy band diagram for the hole injection at both the Al/MoO_x/C_{60} and C_{60}/NPB interfaces. Fig. 5(a) exhibits the Φ_B^h of 1.5 eV between Al anode and pristine C_{60}. As Θ_{MoOx} is increased from 0.4 to 5.0 nm on C_{60}, it is shown that the Φ_B^h can reduce from 1.1 to 0.1 eV. The low Φ_B^h at high Θ_{MoOx} explains that a hole is efficiently injected from the Al anode to the MoO_x/C_{60} layer. Also, as shown in Fig. 5(b), the Φ_B^h from C_{60} to NPB does not

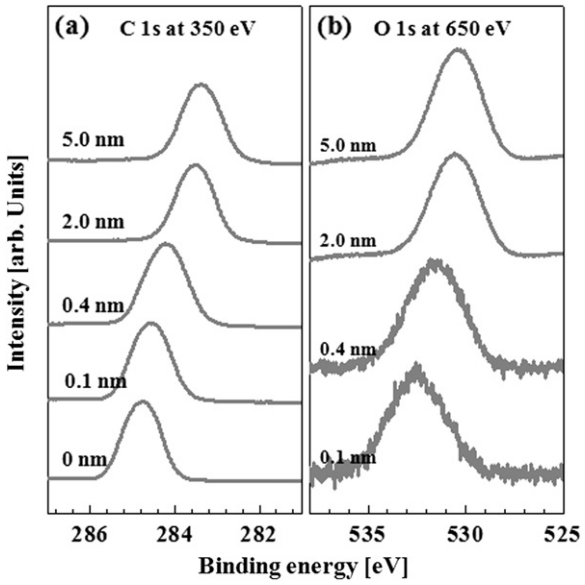

Fig. 2. (a) C 1*s* and (b) O 1*s* XPS core level EDCs measured as a function of Θ_{MoOx} on the 10.0 nm-thick C_{60} layer. The values in the figures indicate the thickness of Θ_{MoOx}.

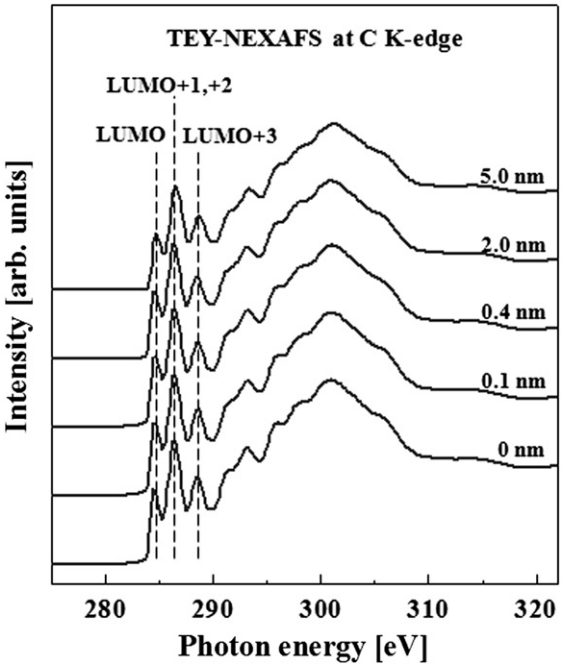

Fig. 3. TEY-NEXAFS spectra at the C K-edge of the MoO_x-on-C_{60} interfaces. The values in the figures indicate the thickness of Θ_{MoOx} on the 10.0 nm-thick C_{60} layer.

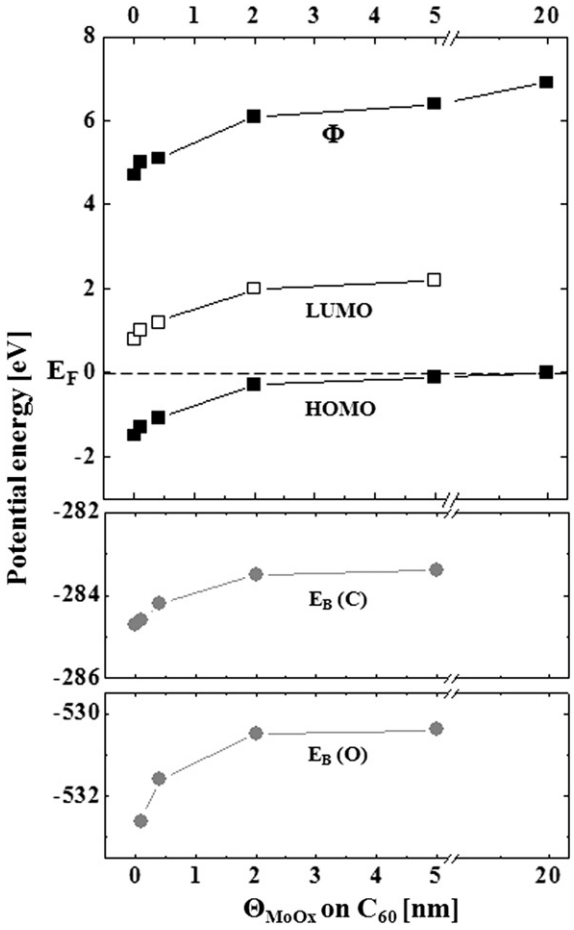

Fig. 4. Energy levels of the MoO_x-on-C_{60} interfaces as a function of Θ_{MoOx} on the 10.0 nm-thick C_{60} layer.

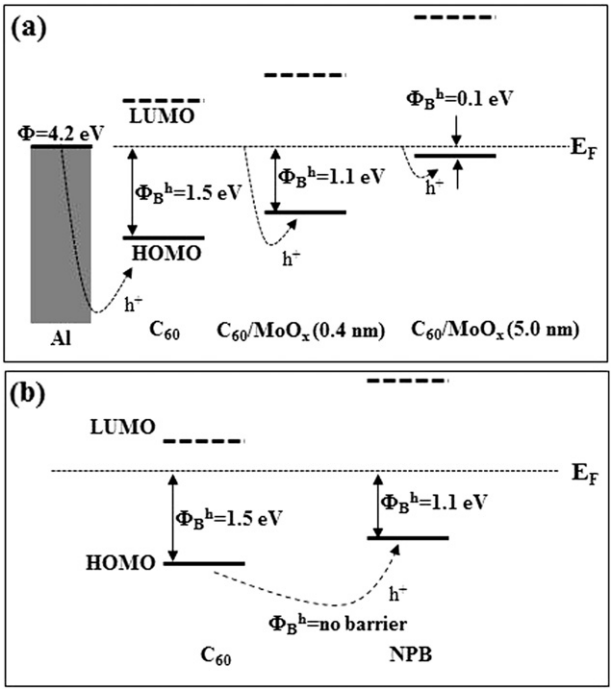

Fig. 5. Proposed energy band diagrams at both the Al/MoO_x/C_{60} (a) and C_{60}/NPB interfaces (b).

exist in the energy band diagram because the HOMO level of C_{60} is higher than that of NPB, thereby expecting an improvement in the hole-injecting property at the Al/MoO_x/C_{60}/NPB interfaces. Moreover, this result proves that the MoO_x-on-C_{60} layers can serve as a potential material to improve a *p*-type contact in inverted TE-OLEDs.

Up to now, the electronic structures of the MoO_x-on-C_{60} interfaces were investigated to apply their interfacial characteristics to inverted TE-OLEDs. The inverted TE-OLEDs composed of a *p*-Si/Al (150 nm)/LiF (1.0 nm)/Alq_3 (40.0 nm)/NPB (60.0 nm)/C_{60} (5.0 nm)/MoO_x (x nm)/Al (2.0 nm)/Ag (18.0 nm)/Alq_3 (52.0 nm) structure which includes the MoO_x-on-C_{60} interfaces were fabricated to study the effect of MoO_x in these MoO_x-on-C_{60} interfaces by measuring the electrical characteristic of the OLEDs. Fig. 6(a) shows the current density–voltage characteristics of the inverted TE-OLEDs, which were obtained to optimize the Θ_{MoOx} on the MoO_x-on-C_{60} layer. The

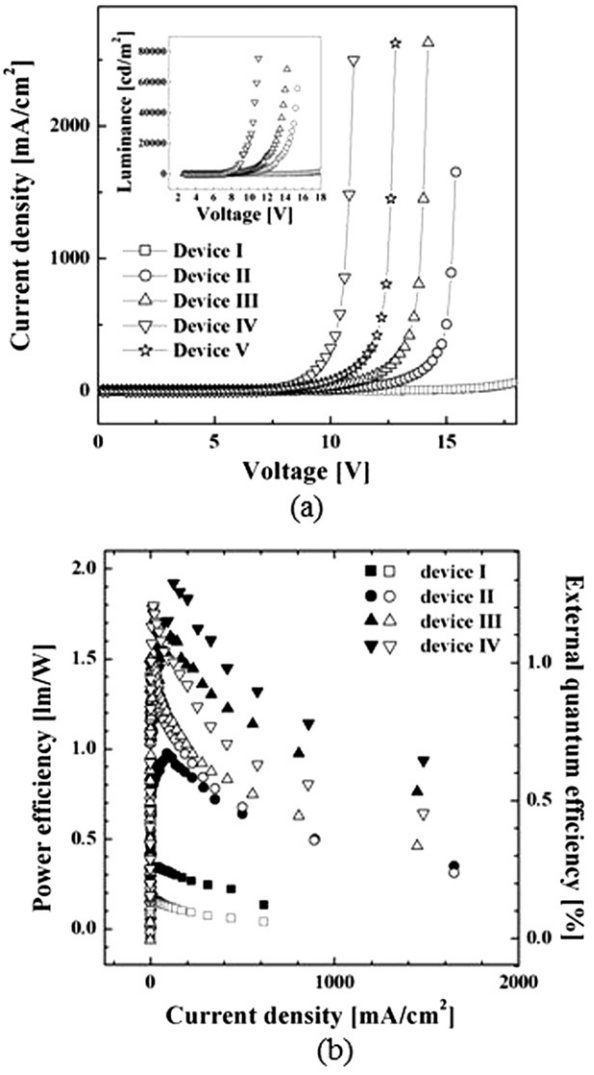

Fig. 6. (a) Current density–voltage characteristics of the inverted TE-OLEDs with various Θ_{MoOx}. The device structure is composed of *p*-Si/Al (150 nm)/LiF (1.0 nm)/Alq_3 (40.0 nm)/NPB (60.0 nm)/C_{60} (5.0 nm)/MoO_x (x nm)/Al (2.0 nm)/Ag (18.0 nm)/Alq_3 (52.0 nm). Here, *x* is 0 (device I), 0.5 (device II), 1.0 (device III), and 5.0 nm (device IV), respectively. The device V has only the sole MoO_x layer of 5 nm-thick instead of the C_{60}/MoO_x layer as a HIL. The inset of Fig. 6(a) shows the luminance as a function of bias voltage in each device. (b) Power efficiency–current density (closed dots) and external quantum efficiency–current density characteristics (open dots) for the devices I, II, III, and IV.

Θ_{MoOx} of the devices I, II, III, and IV were 0, 0.5, 1.0, and 5.0 nm, respectively. As shown in the figure, the device IV with Θ_{MoOx} of 5.0 nm on C_{60} as HTLs exhibited the lowest operating voltage of 7.8 V at the current density of about 20 mA/cm^2. In contrast, the devices with the Θ_{MoOx} of less than 5.0 nm on C_{60} showed higher operating voltages of 16.2, 11.0, and 9.4 eV for the devices I, II, and III, respectively at a constant current density of about 20 mA/cm^2. Also, the device V, which has MoO_x only as a HIL, exhibited 8.2 V of operating voltage which is higher than that of the device IV as shown in Fig. 6(a). It is believed that C_{60} in the C_{60}/MoO_x bilayer structure as the HIL plays an important role in improving the overall injection process through the low Φ_B^h, due to the positive enhanced band bending as explained in Figs. 4 and 5, compared to MoO_x only as the HIL. Meanwhile, the turn-on voltage (V_T) at a luminance of about 0.01 cd/m^2 for the devices I, II, III, and VI were 5.8, 4.2, 3.0, and 2.8 V, respectively. Clearly, at a given luminance, the device IV showed a lower driving voltage than the other three devices. The deriving voltage is significantly decreased as a Θ_{MoOx} is increased, indicating that the interface resistance of the MoO_x-on-C_{60} layer is reduced. In the case of the maximum luminance (L_{max}), the device IV as shown in the inset of Fig. 6(a) showed the highest L_{max} of 76000 cd/m^2 at the voltage of 11.0 V among the devices investigated.

Fig. 6(b) shows both the power efficiency (η_{PE}: closed dots) and external quantum efficiency (η_{EQE}: open dots) measured as a function of the current density of each device. The η_{PE} values at the luminance of 1000 cd/m^2 (L_{1000}) were 0.2 (17.2), 0.8 (10.0), 1.2 (8.8), and 1.7 lm/W (7.6 V), for the devices I, II, II, and IV, respectively. Also, The η_{EQE} values at the luminance of 1000 cd/m^2 (L_{1000}) were 0.1 (17.2), 0.6 (10.0), 0.9 (8.8), and 1.2% (7.6 V), for the devices I, II, II, and IV, respectively. When the device characteristics such as V_T, L_{max}, η_{PE}, and η_{EQE} were compared among the devices in Fig. 6(b), the device IV with the MoO_x (5.0 nm)-on-C_{60} (5.0 nm) also showed the best light-emitting properties. The current density–voltage-luminance characteristics were in well agreement with the reduction of the Φ_B^h in the MoO_x-on-C_{60} layers due to the positive band bending as already shown in Figs. 1 and 2, functioning as a better hole conductor with increasing the Θ_{MoOx} on C_{60}.

4. Conclusions

The interface mechanism of MoO_x-on-C_{60} was originated from the Φ difference due to the band bending, not being occurred from interfacial dipole effect by electron charge transfer. Moreover, TEY-NEXAFS spectra at the C K-edge did not show any structural modification as well as any chemical reaction. In the energy level studies by UPS and XPS, the sign of an Φ shift, HOMO-level shift and core-level shifts (C 1*s* and O 1*s*) were all positive. Therefore, Φ_B^h was reduced to 0.1 eV by simple band bending, with increasing the Θ_{MoOx} to 5 nm on the MoO_x-on-C_{60} interfaces. The characteristics of these electronic structures are in well agreement to the device performance of inverted TE-OLEDs with these interfaces. The optimized device exhibited both the η_{PE} of 1.7 lm/W at the luminance of 1000 cd/m^2 and the L_{max} of 76000 cd/m^2 at the bias voltage of 11.0 V.

Acknowledgments

This work was supported in part by the World Class University program of National Research Foundation of Korea (Grant No. R32-10124) and was supported by the National Research Foundation of Korea Grant funded by the Korean Government (MEST) (NRF-2010-M1AWA001-2010-0026248) and was supported by Pohang Accelerator Laboratory in Korea.

References

[1] K. Leo, Nat. Photonics 5 (2011) 716.
[2] B.W. D'Andrade, S.R. Forrest, Adv. Mater. 16 (2004) 1585.
[3] G. Gustafsson, Y. Cao, G.M. Treacy, F. Klavetter, N. Colaneri, J. Heeger, Nature 357 (1992) 477.
[4] J. Lih, F. Sung, SID'02 DIGEST, 2003, 14.
[5] D.U. Jin, J.K. Jeong, H.S. Shin, M.K. Kim, T.K. Ahn, S.Y. Kwon, J.H. Kwack, T.W. Kim, Y.G. Mo, H.K. Chung, SID'06 DIGEST, 2006 1855.
[6] H. Ishii, K. Sugiyama, E. Ito, K. Seki, Adv. Mater. 11 (1999) 605.
[7] C.-I. Wu, C.-T. Lin, G.-R. Lee, T.-Y. Cho, C.-C. Wu, T.-W. Pi, J. Appl. Phys. 105 (2009) 33717.
[8] T. Matsushima, C. Adachi, J. Appl. Phys. 103 (2008) 54501.
[9] W.-J. Shin, J.-Y. Lee, J.C. Kim, T.-H. Yoon, T.-S. Kim, O.-K. Song, Org. Electron. 9 (2008) 333.
[10] T. Matsushima, Y. Kinoshita, H. Murata, Appl. Phys. Lett. 91 (2007) 253504.
[11] G. Xie, Y. Meng, F. Wu, C. Tao, D. Zhang, M. Liu, Q. Xue, W. Chen, Y. Zhao, Appl. Phys. Lett. 92 (2008) 93305.
[12] C.-C. Chang, M.-T. Hsieh, J.-F. Chen, S.-W. Hwang, C.-H. Chen, Appl. Phys. Lett. 89 (2006) 253504.
[13] X.L. Zhu, J.X. Sun, H.J. Peng, Z.G. Meng, M. Wong, H.S. Kwok, Appl. Phys. Lett. 87 (2005) 153508.
[14] D.-S. Leem, H.-D. Park, J.-W. Kang, J.-H. Lee, J.W. Kim, J.-J. Kim, Appl. Phys. Lett. 91 (2007) 11113.
[15] J.-H. Lee, D.-S. Leem, H.-J. Kim, J.-J. Kim, Appl. Phys. Lett. 94 (2009) 123306.
[16] J. Hou, J. Wu, Z. Xie, L. Wang, Appl. Phys. Lett. 95 (2009) 203508.
[17] Z.Y. Xie, L.S. Hung, F.R. Zhu, Chem. Phys. Lett. 381 (2003) 691.
[18] X. Crispin, V. Geskin, A. Crispin, J. Cornil, R. Lazzaroni, W.R. Salaneck, J.-L. Brédas, J. Am. Chem. Soc. 124 (2002) 8131.
[19] A.J. Maxwell, P.A. Bruhwiler, D. Arvanitis, J. Hasselstrom, Phys. Rev. B 57 (1998) 7312.
[20] I. Hong, M. Lee, Y. Koo, H. Jeong, T. Kim, O. Song, Appl. Phys. Lett. 87 (2005) 063502.
[21] C.C. Chang, J.F. Chen, S.W. Hwang, C.H. Chen, Appl. Phys. Lett. 87 (2005) 253501.
[22] C.-W. Chen, P.-Y. Hsieh, H.-H. Chiang, C.-L. Lin, H.-M. Wu, C.-C. Wu, Appl. Phys. Lett. 83 (2003) 5127.
[23] L.S. Hung, M. Tang, M.G. Mason, P. Raychaudhuri, J. Madathil, Appl. Phys. Lett. 78 (2001) 544.
[24] X.D. Feng, C.J. Huang, V. Lui, R.S. Khangura, Z.H. Lu, Appl. Phys. Lett. 86 (2005) 143511.
[25] A. Opitz, M. Bronner, W. Brütting, Appl. Phys. Lett. 90 (2007) 212112.
[26] H. Li, I. Kurash, F. Liu, Y. Xu, Surf. Sci. 540 (2003) L631.
[27] F. Schiller, M. Ruiz-Osés, J.E. Ortega, B.P. Doyle, V. Pérez-Dieste, J. Lobo, N. Néel, R. Berndt, J. Kröger, J. Chem. Phys. 125 (2006) 144719.